Inflammation Research (2024) 73:47–63
https://doi.org/10.1007/s00011-023-01819-8

Inflammation Research

ORIGINAL RESEARCH PAPER

Tangeretin attenuates acute lung injury in septic mice by inhibiting ROS-mediated NLRP3 inflammasome activation via regulating PLK1/AMPK/DRP1 signaling axis

Yuntao Liu[1] · Yuting Zhang[2] · Guoxing You[2] · Danwen Zheng[1] · Zhipeng He[1] · Wenjie Guo[2] · Kim Antonina[3] · Ziyadullaev Shukhrat[3] · Banghan Ding[1] · Jie Zan[2] · Zhongde Zhang[1]

Received: 23 August 2023 / Revised: 5 October 2023 / Accepted: 6 November 2023 / Published online: 26 December 2023

Abstract

Objective NLRP3 inflammasome-mediated pyroptosis of macrophage acts essential roles in the progression of sepsis-induced acute lung injury (ALI). Tangeretin (TAN), enriched in citrus fruit peel, presents anti-oxidative and anti-inflammatory effects. Here, we aimed to explore the potentially protective effect of TAN on sepsis-induced ALI, and the underlying mechanism of TAN in regulating NLRP3 inflammasome.

Material and methods The effect of TAN on sepsis-induced ALI and NLRP3 inflammasome-mediated pyroptosis of macrophage were examined in vivo and in vitro using a LPS-treated mice model and LPS-induced murine macrophages, respectively. The mechanism of TAN regulating the activation of NLRP3 inflammasome in sepsis-induced ALI was investigated with HE staining, Masson staining, immunofluorescent staining, ELISA, molecular docking, transmission electron microscope detection, qRT-PCR, and western blot.

Results TAN could evidently attenuate sepsis-induced ALI in mice, evidenced by reducing pulmonary edema, pulmonary congestion and lung interstitial fibrosis, and inhibiting macrophage infiltration in the lung tissue. Besides, TAN significantly suppressed inflammatory cytokine IL-1β and IL-18 expression in the serum or bronchoalveolar lavage fluid (BALF) samples of mice with LPS-induced ALI, and inhibited NLRP3 inflammasome-mediated pyroptosis of macrophages. Furthermore, we found TAN inhibited ROS production, preserved mitochondrial morphology, and alleviated excessive mitochondrial fission in LPS-induced ALI in mice. Through bioinformatic analysis and molecular docking, Polo-like kinase 1 (PLK1) was identified as a potential target of TAN for treating sepsis-induced ALI. Moreover, TAN significantly inhibited the reduction of PLK1 expression, AMP-activated protein kinase (AMPK) phosphorylation, and Dynamin related protein 1 (Drp1) phosphorylation (S637) in LPS-induced ALI in mice. In addition, Volasertib, a specific inhibitor of PLK1, abolished the protective effects of TAN against NLRP3 inflammasome-mediated pyroptosis of macrophage and lung injury in the cell and mice septic models.

Conclusion TAN attenuates sepsis-induced ALI by inhibiting ROS-mediated NLRP3 inflammasome activation via regulating PLK1/AMPK/DRP1 signaling axis, and TAN is a potentially therapeutic candidate against ALI through inhibiting pyroptosis.

Keywords Sepsis · Acute lung injury · NLRP3 inflammasome · Polo-like kinase 1 · Dynamin related protein 1

Introduction

Sepsis-induced ALI is a life-threatening organ dysfunction, which is the major cause of admission and death in hospital intensive care units [1]. Numerous studies report that sepsis-induced ALI is closely associated with diffuse inflammatory cell infiltration, followed with uncontrolled inflammatory responses, alveolar-capillary barrier damage, and pulmonary physiological dysfunction [2, 3]. Although great achievements have been made in lung-protective mechanical ventilation, prone positioning, and extracorporeal membrane

Responsible Editor: Anatolii Kubyshkin.

Yuntao Liu and Yuting Zhang have contributed equally to this work and share first authorship.

Extended author information available on the last page of the article

oxygenation, the mortality rate of sepsis-induced ALI is still high [4, 5]. Therefore, developing effective pharmacotherapies for sepsis-induced ALI is urgently needed.

Macrophages are the major leukocyte population of innate immune cells infiltrating into the lungs in sepsis and ALI, and play essential roles in producing pro-inflammatory factors [6, 7]. Suppression of macrophages-mediated excessive inflammatory response could evidently improve pulmonary function and survival status in sepsis [8–10]. Recently, more and more studies report that pyroptosis, a pro-inflammatory type of regulated cell death, acts an important role in the pathogenesis of sepsis and ALI [11–13]. Generally, pyroptosis is usually triggered by assemble inflammasomes which promote the formation of active caspase-1 via the adaptor protein apoptosis-associated speck-like protein containing a caspase recruitment domain (ASC), and then lead to cleave gasdermin D (GSDMD) and release of interleukin-1β (IL-1β) and IL-18 [14–16]. Among the pyroptosis-related inflammasomes, nucleotide-binding domain, leucine-rich repeat-containing receptor, pyrin domain-containing-3 (NLRP3) inflammasome-mediated pyroptosis is the most widely studied, and is closely involved in sepsis and ALI [17, 18]. Fully clarifying the regulatory mechanism of NLRP3 inflammasome-mediated pyroptosis is essential for developing the effective pharmacotherapies for sepsis-induced ALI.

Mitochondria, which are dynamic organelles, not only play important roles in energy production but also are closely involved in apoptosis and inflammasome activation [19]. The balance of mitochondrial dynamics is essential for mitochondrial function, and the disturbance of mitochondrial fusion and division induces overloaded mitochondrial reactive oxygen species (ROS) production, injured mitochondrial proteins and DNA, resulting in the activation of NLRP3 inflammasome [20–22]. Mitochondrial fission is regulated by Dynamin related protein 1 (Drp1) and its mitochondrial adaptor fission 1 (Fis1), and excessive fission leads to mitochondrial fragmentation and dysfunction [23, 24]. Recent studies report that mitochondrial dysfunction acts essential roles in the pathogenesis of sepsis and ALI [25], and dexmedetomidine, hydrogen, and Kahweol have been identified to alleviate sepsis-induced ALI via regulating mitochondrial dynamics [26–28]. Thus, mitochondrial dynamics represents a powerful therapeutic target for sepsis-induced ALI therapy.

Nowadays, plant-derived natural products have attracted more and more attention for sepsis and ALI, owing to their valuable biological activities and low side effects. Tangeretin (TAN) is a natural polymethoxyflavone compound abundant in citrus fruit peel, and has multiple biological functions such as anti-viral, anti-cancer, anti-oxidation, and anti-inflammation [29–31]. TAN inhibits inflammatory response in osteoarthritis through regulating the MAPK/NF-κB signaling pathways [31]. TAN alleviates hepatic steatosis and oxidative stress in high fat diet-induced nonalcoholic fatty liver disease via regulating Nrf2 pathway [32]. Recently, TAN has been found to protect sepsis-induced myocardial dysfunction via regulating the PTEN/AKT/mTOR axis [33]. However, whether TAN protects sepsis-induced ALI and its underlying mechanism is completely unknown.

In the present study, we analyzed the effects of TAN on sepsis-induced ALI using a LPS-induced sepsis model. Furthermore, we explored the protective mechanism of TAN attenuating sepsis-induced ALI in vivo an in vitro. To the best of our knowledge, this is the first study indicating the protective effect of TAN on sepsis-induced ALI through inhibiting macrophage pyroptosis via the PLK1-AMPK-Drp1-NLRP3 axis.

Material and methods

Mice model of sepsis-induced ALI

The study protocol is approved by the Institutional Animal Care and Use Committee of Guangdong Provincial Hospital of Traditional Chinese Medicine (No. 2023017). Male C57BL/6 mice (6–8 weeks old) were purchased from the GemPharmatech Co., Ltd (Nanjing, China), and were housed in a room kept at 24 ± 2 °C temperature and approximately 40% humidity in a 12 h dark/12 h light cycle, and had free access to standard food and water. Sepsis-induced ALI was established using 10 mg/kg LPS (Sigma-Aldrich, USA) via intraperitoneal injection. TAN (50 mg/kg, B20646, ShanghaiyuanyeBio, China) or an equal amount of vehicle was intraperitoneally injected into mice 30 min before LPS administration. The dose of TAN was based on previous study [34].To explore the protective role of TAN for sepsis-induced ALI, 24 mice were randomly divided into Sham groups ($n = 6$), TAN ($n = 6$), LPS ($n = 6$), and LPS + TAN ($n = 6$). To investigate whether PLK1 is involved in the TAN's protective effect, 24 mice were divided into four groups, including Sham group ($n = 6$), LPS group ($n = 6$), LPS + TAN (50 mg/kg) group ($n = 6$), and LPS + TAN + Volasertib (S2235, Selleck, USA) group ($n = 6$). Volasertib (20 mg/kg), a specific inhibitor of PLK1, was intraperitoneally injected into the mice 30 min before TAN administration. After 12 h of LPS stimulation, mice were euthanized to collect the lung bronchoalveolar lavage fluid (BALF), and lung tissue samples.

Hematoxylin–eosin (HE) staining and Masson staining

HE staining and Masson staining were performed as previously described [35, 36].

Calculation of weight loss rate

Weight loss is calculated as: weight loss rate = | (the weight of mice before execution-the weight of mice before intervention)/the weight of mice before intervention |× 100%.

Calculation of lung wet–dry weight ratio

After execution, mice fresh lungs were excised and then weighed to obtain the wet (W) weight and the dry (D) weight before and after desiccation at 80 °C for 24 h, respectively. Lung W/D weight ratio is calculated as: Lung W/D weight ratio = the W weigh/the D weight.

Calculation of lung injury scores

Lung injury scores were independently assessed and were scored by the Mikawa method [37]. Briefly, a semi-quantitative analysis of lung injury in mice was performed, according to the following criteria: (1) alveolar hemorrhage; (2) alveolar edema; (3) infiltration or aggregation of neutrophils in the alveolar or vascular; (4) alveolar wall thickening and/or hyaline membrane. Briefly, the histological changes were scored on a scale of 0–4 (0, normal; 1, mild; 2, moderate; 3, severe; 4, intense). A cumulative histology score for all parameters was calculated.

Enzyme-linked immunosorbent assay (ELISA)

The expression levels of inflammatory cytokines, tumor necrosis factor-α (TNF-α) and interleukin-1β (IL-1β) in the mice serum or the BALF were examined using the Mouse TNF-α ELISA Kit (EK282, Multi-Sciences, Hangzhou, China), and the Mouse IL-1β High Sensitivity ELISA Kit (EK201BHS, Multi-Sciences, Hangzhou, China), respectively, according to the manufacturer's protocol.

Cell culture

Primary peritoneal macrophages were isolated from the C57BL/6 mice which were injected with 1 ml of 3% Brewer thioglycollate medium into the peritoneal cavity for 4 days. Then, 10 ml of PBS was administrated to the peritoneal cavity of the mouse, and peritoneal fluid was collected into a 50 ml tube and centrifuged to obtain the peritoneal exudate cells. Finally, the supernatant was removed, and cell pellet was resuspended in DMEM and kept in a CO_2 incubator at 37 °C for 24 h for subsequent cell experiments. Primary peritoneal macrophages were stimulated with DMSO or TAN (2.5 μM) for 1 h, and then treated with 500 ng/mL LPS for 5.5 h before 2 mM ATP (BS215, Biosharp, China) was supplied for an additional 30 min. To investigate whether ROS is involved in the TAN's protective effect in vitro, peritoneal macrophages were treated with the ROS inducer Rotenone (250 nM, S2348, Selleck, USA) 60 min before TAN treatment. To investigate whether PLK1 is involved in the TAN's protective effect in vitro, peritoneal macrophages were treated with Volasertib (10 nM, S2235, Selleck, USA) 60 min before TAN treatment.

Immunofluorescence

After deparaffination, rehydration, and antigen retrieval, lung tissue sections at thickness of 5 μm were blocked with 5% BSA, stained with the primary antibodies, and then stained with the secondary antibodies, as previously described [38]. The primary antibodies, including F4/80 antibody (sc-52664, Santa Cruz, USA), ASC antibody (ab309497, Abcam, USA), GSDMD (20770-1-AP, Proteintech), PLK1 antibody (10305-1-AP, Proteintech), Phospho-DRP1 (Ser637) antibody (AF5791, Beyotime), and NLRP3 (68,102-1-Ig, Proteintech) were used.

Screening targets for TAN

The 2D structure of TAN was obtained from MolView (http://molview.org/), and then imported into the Swiss Target Prediction database (http://www.swisstargetprediction.ch/) to obtain the potential target genes. ALI-related genes, and organelle biogenesis and maintenance-related genes were obtained from the GeneCards (https://auth.lifemapsc.com/), respectively. Then, the intersected genes were obtained by Venn diagram analysis (http://www.ehbio.com/test/venn/#/). The TAN and potential protein targets were subjected to molecular docking using AutoDock 4.0 software. A binding energy of − 5.0 kcal/mol was defined as having potential binding affinity.

Western blotting

Lung tissues were collected, lysed, quantified with BCA protein assay kit (P0010S, Beyotime), separated with 12% SDS-PAGE gels, transferred onto nitrocellulose membranes, and then subjected to immunoblot analysis, as our previously described [38]. The antibodies against NLRP3 (68102-1-Ig, Proteintech), GSDMD (20770-1-AP, Proteintech), PLK1 antibody (10305-1-AP, Proteintech), AMPK antibody (10305-1-AP, 10929-2-AP), Phospho-AMPK (Thr172) antibody (AF3423, Affinity), Phospho-DRP1 (Ser637) antibody (AF5791, Beyotime), DRP1 antibody (12957-1-AP, Proteintech), Caspase1 antibody (81482-1-RR, Proteintech), and β-actin (81115-1-RR, Proteintech) were used.

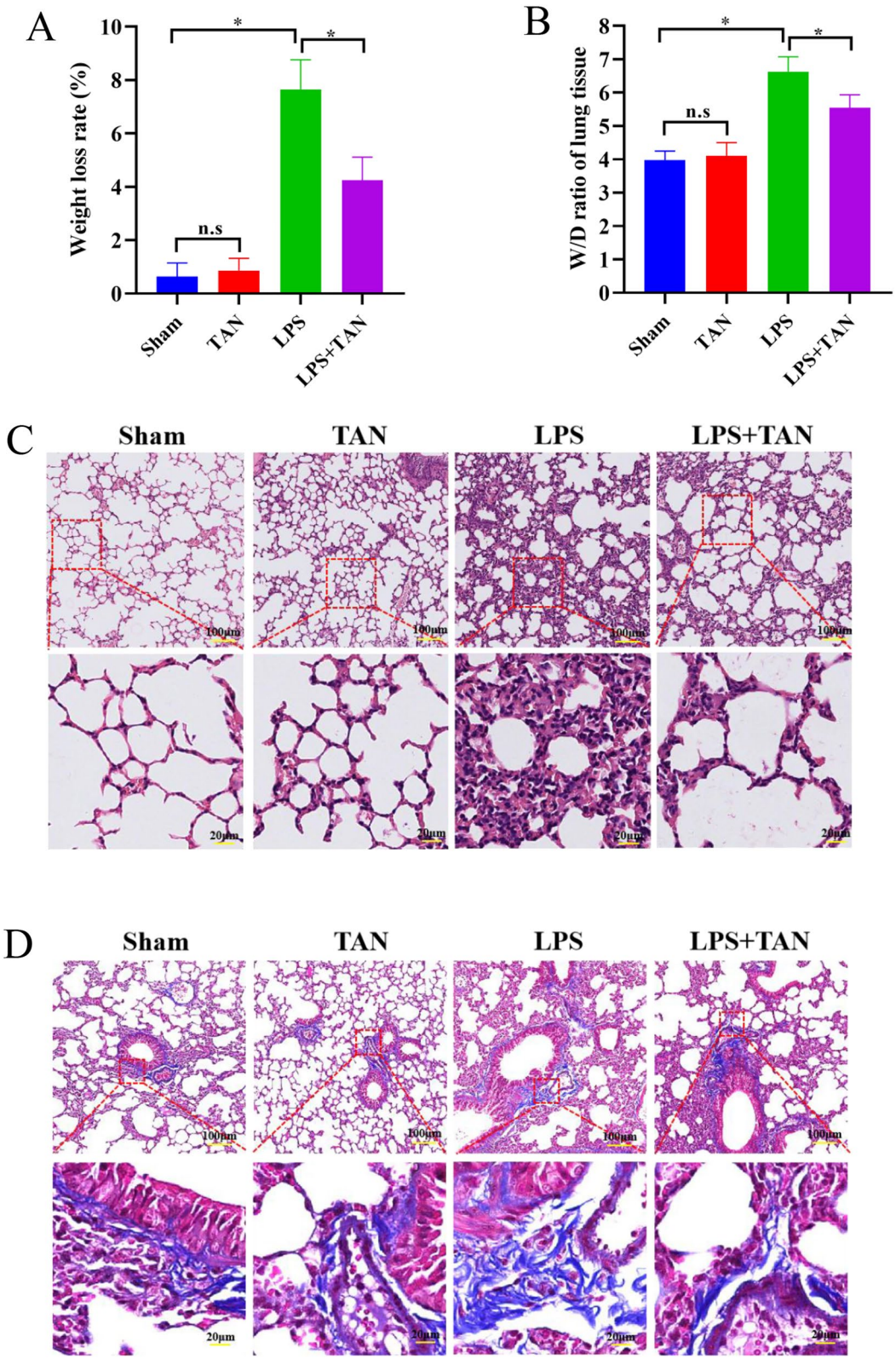

Fig. 1 TAN attenuates LPS-induced ALI in mice. **A** Mice weight loss ratio was determined in all groups ($n=6$). **B** Lung wet-to-dry weight ratio and was determined in all groups ($n=6$). **C** HE staining analysis of lung tissues. **D** Masson staining analysis of lung tissues. Data are represented as mean ± SD, $*p<0.05$

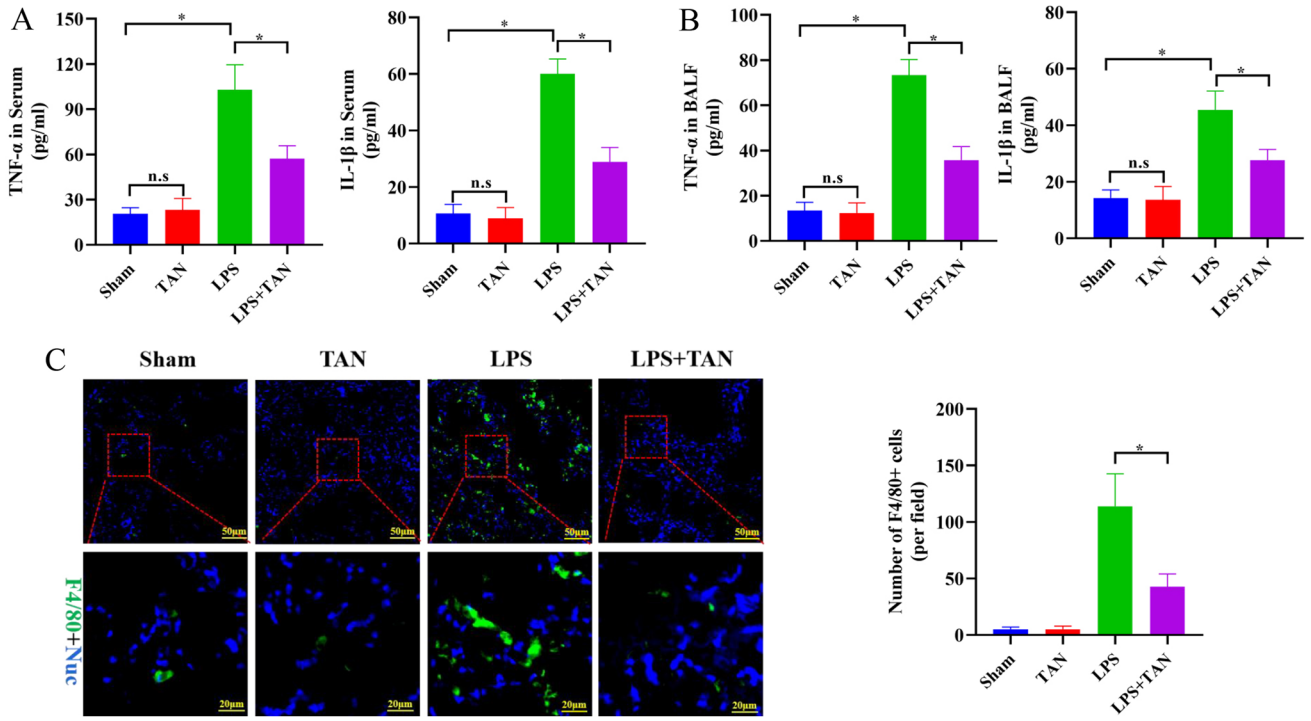

Fig. 2 TAN attenuates inflammatory cytokine expression and inflammatory cell infiltration in mice with LPS-induced lung injury. **A** ELISA detection of TNF-α and IL-1β expression in the serum of all groups ($n=6$). **B** ELISA detection of TNF-α and IL-1β expression in the BALF samples of all groups ($n=6$). **C** Immunofluorescence staining analysis of the macrophage marker F4/80 (green) in the lung injury of all groups ($n=6$). Nucleus was stained with DAPI (blue). The quantification analysis of F4/80-positive cells in lung tissues. Data are represented as mean ± SD, $^*p<0.05$ (color figure online)

Quantitative real-time PCR (qRT-PCR)

Total RNA of the lung tissues or the cells was extracted, inversely transcribed into cDNA, and then performed for qRT-PCR, as our previously described [38]. qRT-PCR primers were as follows: NLRP3, 5′-ATTACCCGCCCG AGAAAGG-3′ and 5′-TCGCAGCAAAGATCCACACAG-3′; IL-1β, 5′-GCAACTGTTCCTGAACTCAACT-3′ and 5′-ATCTTTTGGGGTCCGTCAACT-3′; IL-18, 5′-CCT ACTTCAGCATCCTCTACTGG-3′ and 5′-AGGGTTTCT TGAGAAGGGGAC-3′, and GAPDH, 5′-TCAACAGCA ACTCCCACTCTTCCA-3′ and 5′-CCCTGTTGCTGTAGC CGTATTCA-3′.

ROS detection

ROS levels in the frozen lung sections was detected using the DHE staining kit (BB-470515, Bestbio, China), and mitochondrial ROS levels in the primary peritoneal macrophages were detected using the MitoSOX Red staining kit (40778ES50, YEASEN, China), according to the manufacturer's protocol, respectively. Then, the images were obtained under a fluorescence microscope (LSM880, ZEISS, Germany).

Transmission electron microscope (TEM) detection

TEM was performed as our previously described [39]. Briefly, small pieces of lung samples were fixed in 2.5% glutaraldehyde at least 2 h, washed with PBS for 15 min for total three times, then dehydrated in acetone of different concentrations and saturated with resin overnight. Lung sections (70 nm) were cut and stained with both uranyl acetate and lead citrate. Images were finally acquired by H-7650 (Hitachi, Tokyo, Japan).

JC1 staining

The mitochondrial membrane potential of primary peritoneal macrophages was detected using the JC-1 staining kit (C2006, Beyotime, China), according to the manufacturer's protocol. The cells were observed and photographed (LSM880, ZEISS, Germany).

Statistical analysis

Data were analyzed using the GraphPad Prism 5.0 software (GraphPad Software Inc.) Differences between groups were analyzed by the Student's *t* test or one-way analysis of

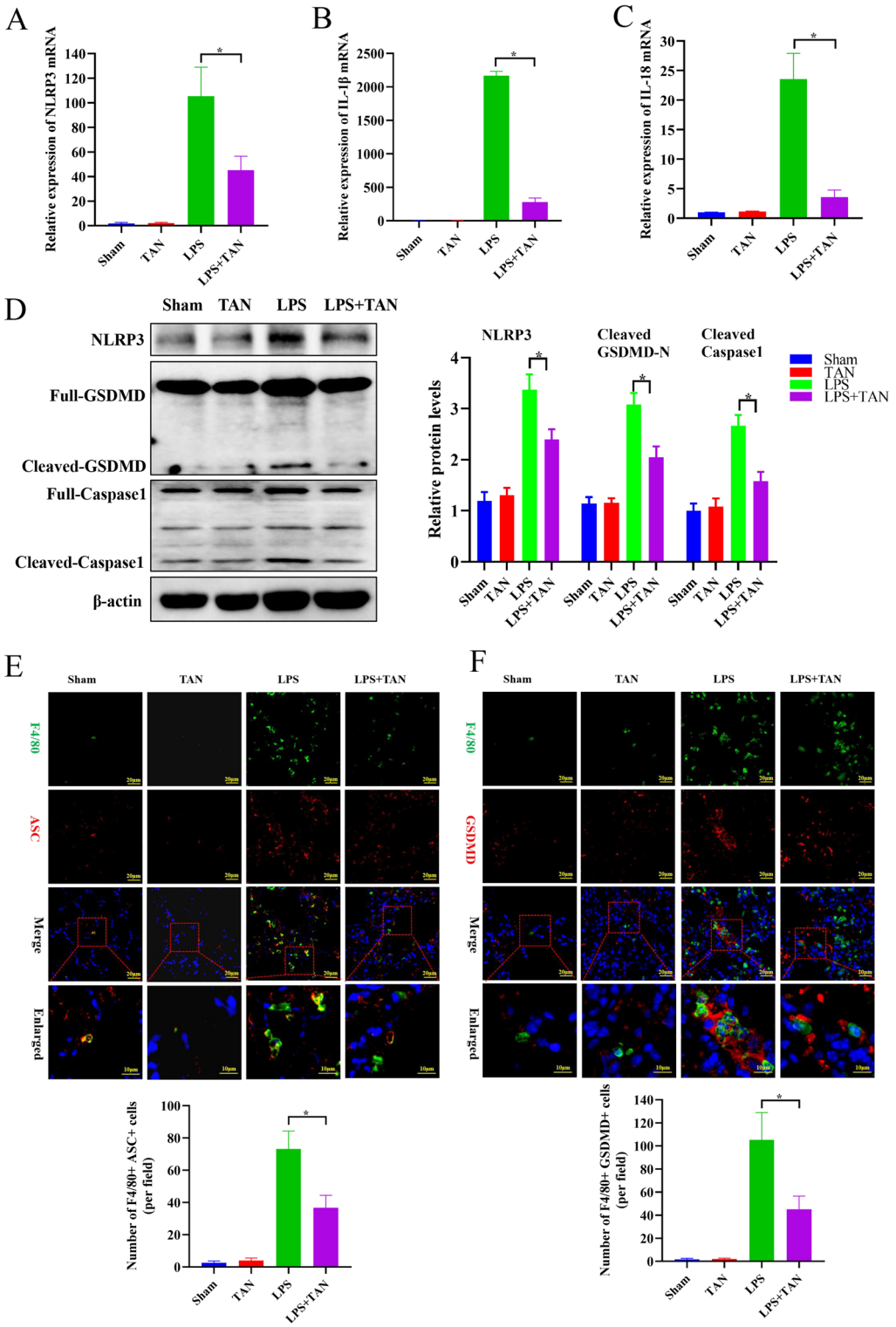

Fig. 3 TAN inhibits NLRP3 inflammasome-mediated-macrophage pyroptosis in LPS-induced ALI in mice. **A**–**C** qRT-PCR analysis of NLRP3, IL-1β and IL-18 mRNA expressions in the lung tissues ($n=3$). **D** Western blotting analysis of NLRP3, cleaved GSDMD, and cleaved Caspase-1 protein expressions in the lung tissues. Quantitative analysis of the indicated protein expressions in the lung tissues ($n=3$). **E** Immunofluorescence staining analysis of the macrophage marker F4/80 (green) and ASC (red) in the lung injury of all groups. Nucleus was stained with DAPI (blue). The quantification analysis of F4/80 and ASC-positive cells in lung tissues ($n=6$). **F** Immunofluorescence staining analysis of the macrophage marker F4/80 (green) and GSDMD (red) in the lung injury of all groups. Nucleus was stained with DAPI (blue). The quantification analysis of F4/80 and GSDMD-positive cells in lung tissues ($n=6$). Data are represented as mean ± SD, $*p<0.05$ (color figure online)

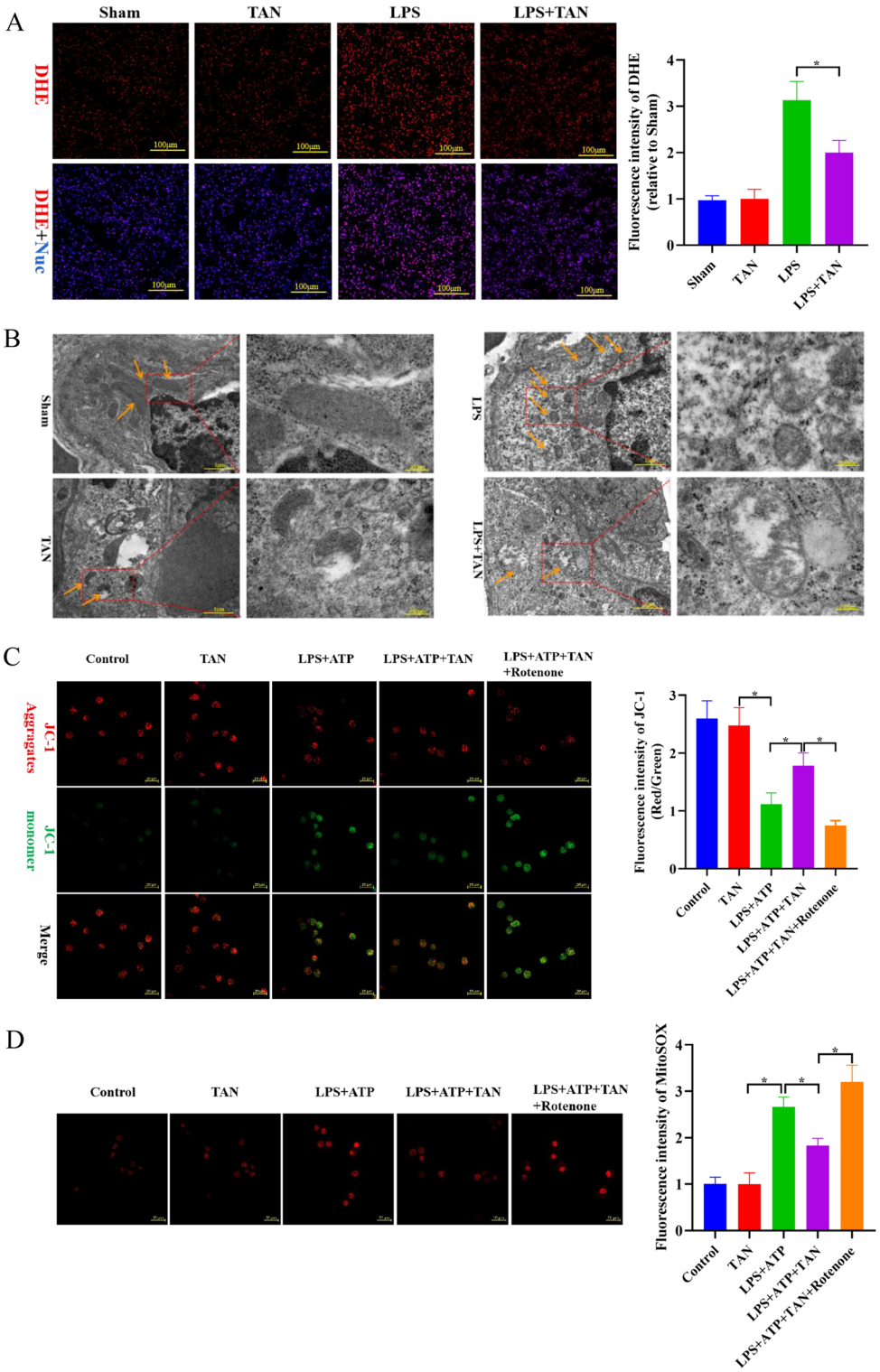

Fig. 4 TAN inhibits ROS production and protects mitochondrial dynamics in LPS-induced ALI in mice. **A** Immunofluorescence staining analysis of DHE (red) in the lung injury of all groups. Nucleus was stained with DAPI (blue). Quantitative analysis of the immunofluorescence intensity of DHE ($n=6$). **B** TEM analysis of the mitochondrial morphology in the lung tissues of all groups. Orange arrow indicates the representative mitochondria. **C** Immunofluorescence staining analysis of JC-1 in the peritoneal macrophages. Quantitative analysis of the immunofluorescence intensity of JC-1 ($n=6$). **D** Immunofluorescence staining analysis of MitoSOX in the peritoneal macrophages. Quantitative analysis of the immunofluorescence intensity of MitoSOX ($n=6$). Data are represented as mean ± SD, $^*p<0.05$ (color figure online)

variance (ANOVA)/Bonferroni multiple-comparison post hoc test. p values (represented by asterisks), where $^*p<0.05$.

Results

TAN attenuates LPS-induced ALI in mice

We firstly explored the potential protective role of TAN on LPS-induced lung injury, and found the weight loss of the

mice in the LPS group was significantly higher than that in the Sham group or the TAN group (Fig. 1A). While, TAN treatment notably attenuated LPS-induced weight loss in the LPS + TAN group (Fig. 1A). Besides, we evaluated pulmonary edema via detecting lung W/D ratio, and found that TAN treatment efficiently suppressed LPS-induced the increase of lung W/D ratio (Fig. 1B). Similarly, HE staining analysis showed that TAN treatment notably protected lung histomorphology in the mice with LPS-induced ALI, as evidenced by reducing pulmonary congestion, thickening of the alveolar wall and leukocyte accumulation (Fig. 1C). The scores for lung injury corresponded to these results (Supplementary Fig. 1A). Moreover, Masson staining analysis showed that TAN treatment also evidently alleviated lung interstitial fibrosis induced by LPS (Fig. 1D; Supplementary Fig. 1B). Collectively, these results indicate TAN could evidently attenuate sepsis-induced ALI in mice.

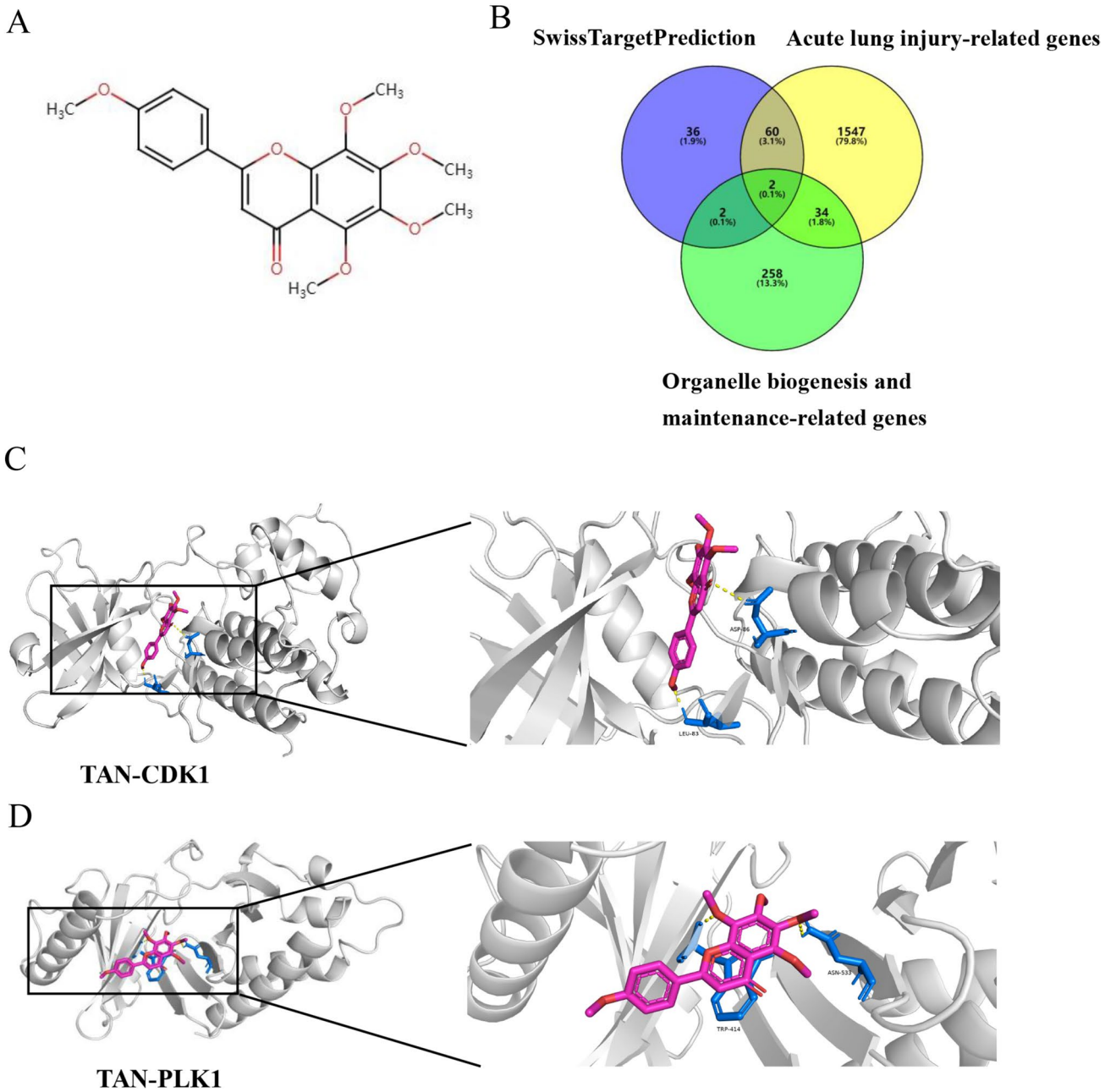

Fig. 5 PLK1 is a potential target of TAN for treating sepsis-indued ALI. **A** Chemical structure of TAN. **B** Venn diagram. **C** Molecular docking models of TAN and CDK1 protein. **D** Molecular docking models of TAN and PLK1 protein

TAN attenuates inflammatory cytokine expression and inflammatory cell infiltration in mice with LPS-induced lung injury

Owing to inflammation acts essential roles in the pathogenesis of sepsis-induced ALI [2, 3], we further examined the expression levels of inflammatory cytokines, and found that TNF-α and IL-1β levels in the serum or BALF samples of LPS group were significantly increased, compared to those in the Sham group or the TAN group (Fig. 2A, B). TAN treatment notably reversed LPS-induced inflammatory cytokines in the LPS + TAN group (Fig. 2A, B). Furthermore, immunofluorescence analysis of the macrophage marker F4/80 in the mice lung tissues, and showed that TAN treatment could significantly inhibit LPS-induced macrophage infiltration in lung tissue (Fig. 2C).

TAN inhibits NLRP3 inflammasome-mediated-macrophage pyroptosis in LPS-induced ALI in mice

Given that NLRP3 inflammasome-mediated pyroptosis is an inflammatory cell death, and acts an important role in the pathogenesis of sepsis-induced ALI [17, 18], we further investigated whether the protective effect of TAN against sepsis-induced ALI is related to regulating NLRP3 inflammasome. As shown in Fig. 3A–C, the mRNA expression levels of NLRP3 and its downstream genes IL-1β and IL-18 were significantly increased in the lung tissues of LPS group, compared to those in the Sham group or the TAN group. However, TAN treatment evidently inhibited these gene expressions in the LPS + TAN group (Fig. 3A–C). Furthermore, Western blotting analysis also showed that TAN treatment evidently inhibited the protein expressions of NLRP3, the cleaved GSDMD which is a surrogate marker of pyroptosis, and the cleaved Caspase-1 in the LPS + TAN group, compared to those in the LPS group (Fig. 3D). Moreover, immunofluorescence analysis showed that TAN treatment significantly inhibited macrophage ASC and GSDMD expressions in the lung tissues of LPS + TAN group, compared to the LPS group (Fig. 3E, F), which further confirms that TAN inhibits NLRP3 inflammasome-mediated-macrophage pyroptosis in LPS-induced ALI in mice.

TAN inhibits ROS production and protects mitochondrial dynamics in LPS-induced ALI in mice

Considering that ROS is a crucial stimuli for the activation of NLRP3 inflammasome [40], and dysfunction of mitochondria could produce huge amount of ROS [41], we further explored whether the protective effect of TAN against NLRP3 inflammasome activation in sepsis-induced ALI is related to regulating ROS production. As shown in Fig. 4A, the ROS levels detected by DHE staining in the lung tissues of the LPS group were significantly increased, compared to those in the Sham group or the TAN group. TAN treatment evidently inhibited ROS production-induced by LPS in the LPS + TAN group (Fig. 4A). Furthermore, we detected the mitochondrial morphology in the lung tissues by TEM, and found that mitochondria were swollen, and round-shaped with smaller size and disrupted mitochondrial cristae in the LPS group, compared to those in the Sham group or the TAN group (Fig. 4B). Whereas, mitochondria were less swollen with elongated appearance and well-organized cristae in the LPS + TAN group, indicating that TAN preserves mitochondrial morphology and alleviates excessive mitochondrial fission in LPS-induced ALI in mice.

Moreover, we explored the protective effect of TAN on mitochondria in the peritoneal macrophages stimulated with LPS and ATP to induce pyroptosis. As shown in the supplementary Fig. 2, 2.5 μM TAN did not evidently influence the cell viability. Subsequently, we found that 2.5 μM TAN treatment significantly suppressed LPS + ATP-induced the depression of mitochondrial membrane potential detected using JC-1 staining and the accumulation of mitochondrial ROS detected using MitoSOX staining (Fig. 4C, D). However, the ROS activator Rotenone treatment notably reversed the protective effects of TAN on the decline of mitochondrial membrane potential dysfunction and mitochondrial ROS accumulation (Fig. 4C, D).

PLK1 is a potential target of TAN for treating sepsis-indued ALI

To clarify the molecular mechanism of TAN protecting mitochondrial morphology in sepsis-induced ALI, we obtained the 2D structure of TAN from MolView (http://molview.org/) (Fig. 5A), and then identified 100 potential target genes of TAN using SwissTargetPrediction database (Supplementary Table 1). Furthermore, 1643 ALI-related genes, and 296 organelle biogenesis and maintenance-related genes were obtained from the GeneCards, respectively (Supplementary Table 1). Through intersecting analysis, cyclin-dependent kinase 1 (CDK1) and PLK1 genes were identified (Fig. 5B). Moreover, the docking energy between TAN and CDK1 or PLK1 was − 7.72 kcal/mol and − 7.06 kcal/mol, respectively, which were both less than − 5.0 kcal/mol, indicating that TAN presents strong binding to CDK1 and PLK1. The binding mode of TAN and CDK1 or PLK1 was visualized by PyMoL (Fig. 5C, D).

Recent studies report that AMPK activation inhibits mitochondrial fission by promoting Drp1 phosphorylation (Ser-637) to attenuate vascular calcification in chronic kidney disease [42], myocardial ischemia–reperfusion injury [43], and allergic rhinitis [44]. PLK1 is identified to promote cholesterol efflux and alleviate atherosclerosis by regulating

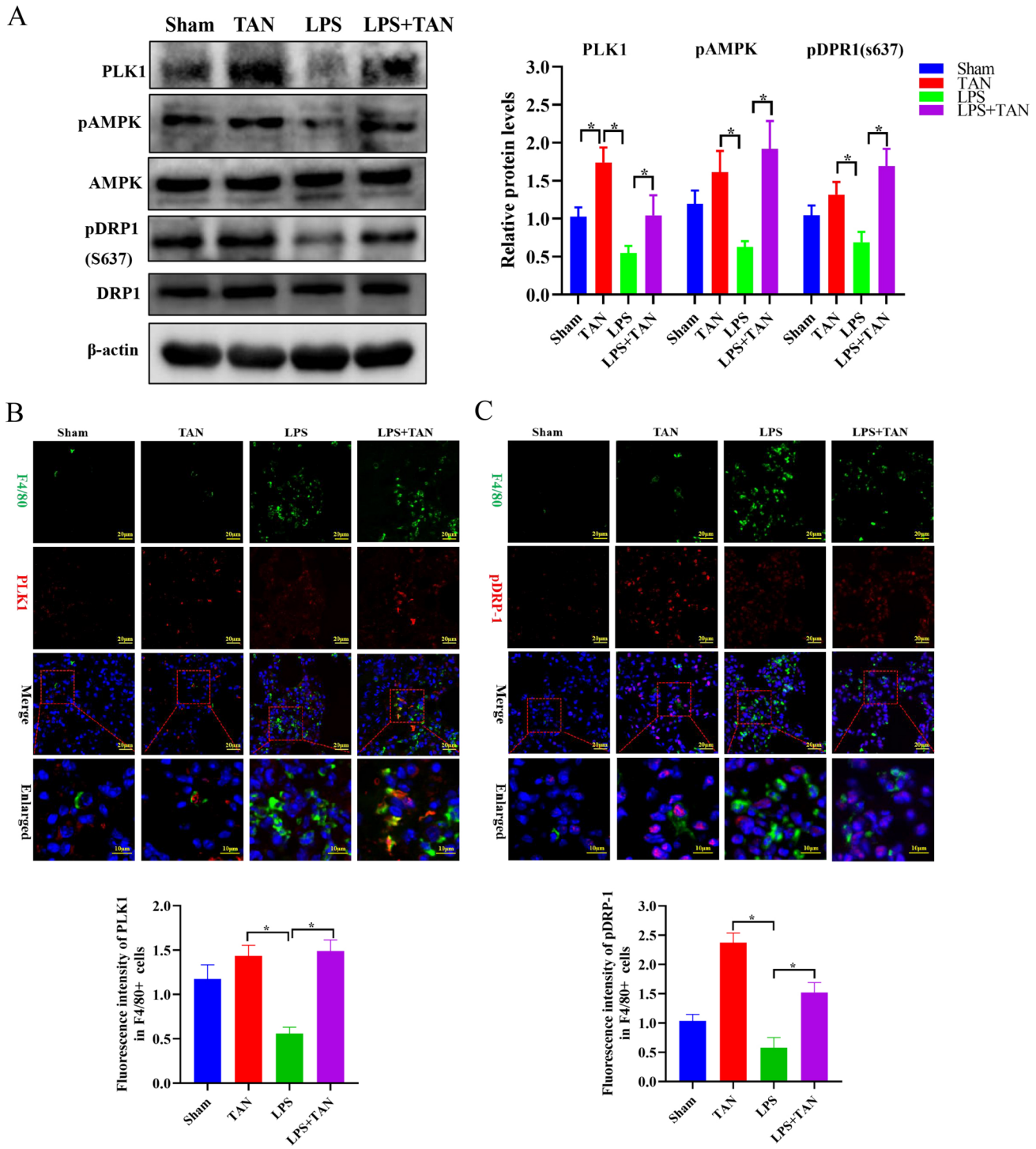

Fig. 6 TAN promotes PLK1-AMPK-Drp1 signaling in LPS-induced ALI in mice. **A** Western blotting analysis of PLK1, phosphorylated AMPK (pAMPK), AMPK, phosphorylated Drp1 (S637) (pDRP1), and DRP1 protein expressions in the lung tissues. Quantitative analysis of the indicated protein expressions in the lung tissues ($n=3$). **B** Immunofluorescence staining analysis of the macrophage marker F4/80 (green) and PLK1 (red) in the lung injury of all groups. Nucleus was stained with DAPI (blue). The quantification analysis of the immunofluorescence intensity of PLK1 in the F4/80-positive cells in lung tissues ($n=6$). **C** Immunofluorescence staining analysis of the macrophage marker F4/80 (green) and pDRP1 (red) in the lung injury of all groups. Nucleus was stained with DAPI (blue). The quantification analysis of the immunofluorescence intensity of pDRP1 in the F4/80-positive cells in lung tissues ($n=6$). Data are represented as mean ± SD, $^*p<0.05$ (color figure online)

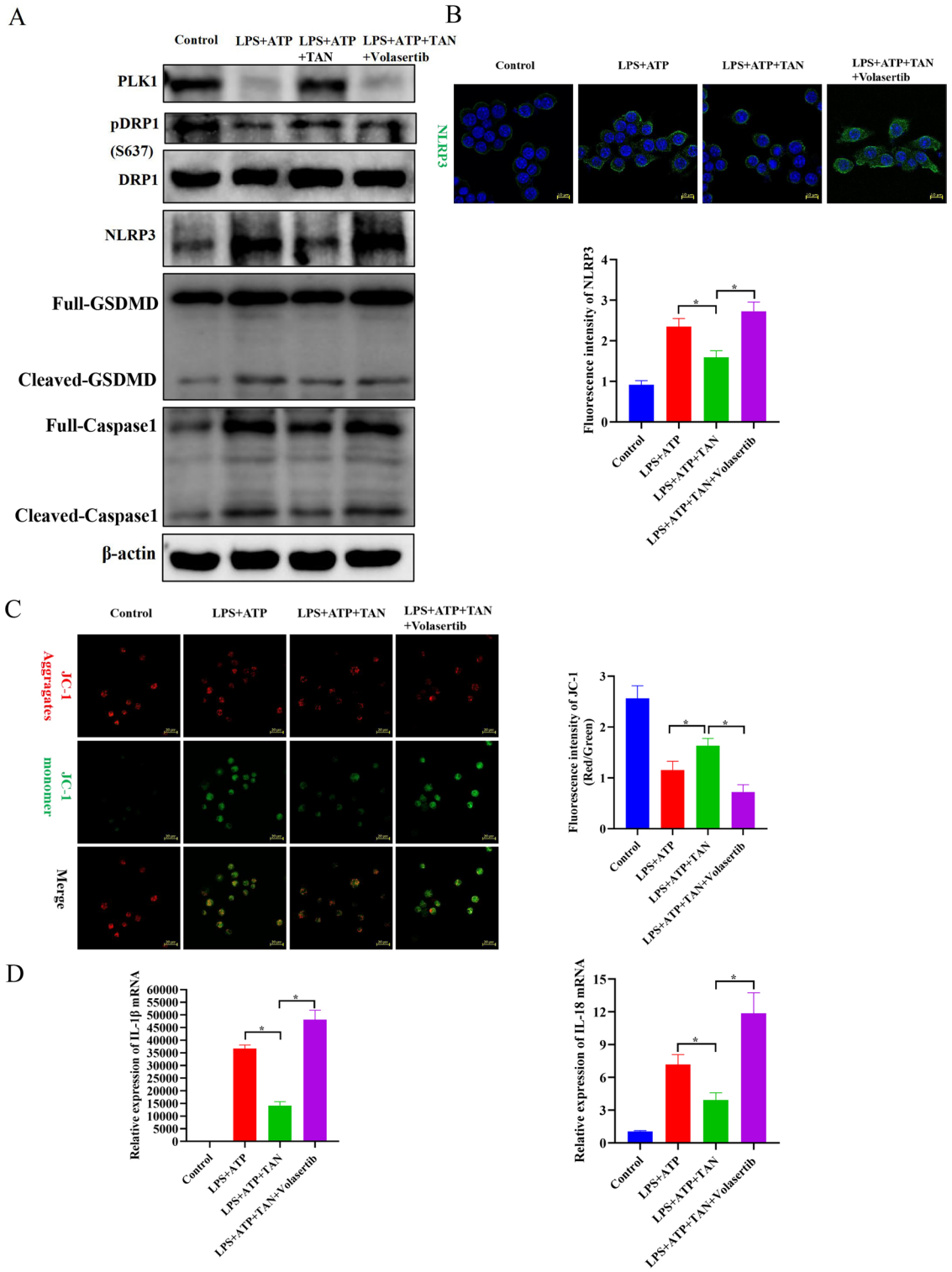

Fig. 7 TAN suppresses NLRP3 inflammasome activation via regulating PLK1-Drp1 signaling in peritoneal macrophages stimulated with LPS and ATP. **A** Western blotting analysis of PLK1, pDRP1, DRP1, NLRP3, GSDMD, and Caspase-1 protein expressions in the peritoneal macrophages. **B** Immunofluorescence staining analysis of NLRP3 (green) in the peritoneal macrophages. Nucleus was stained with DAPI (blue). The quantification analysis of the immunofluorescence intensity of NLRP3 in the peritoneal macrophages ($n=6$). **c** Immunofluorescence staining analysis of JC-1 in the peritoneal macrophages. Quantitative analysis of the immunofluorescence intensity of JC-1 ($n=6$). **D** qRT-PCR analysis of IL-1β and IL-18 mRNA expressions in the peritoneal macrophages ($n=3$). Data are represented as mean ± SD, $^*p<0.05$ (color figure online)

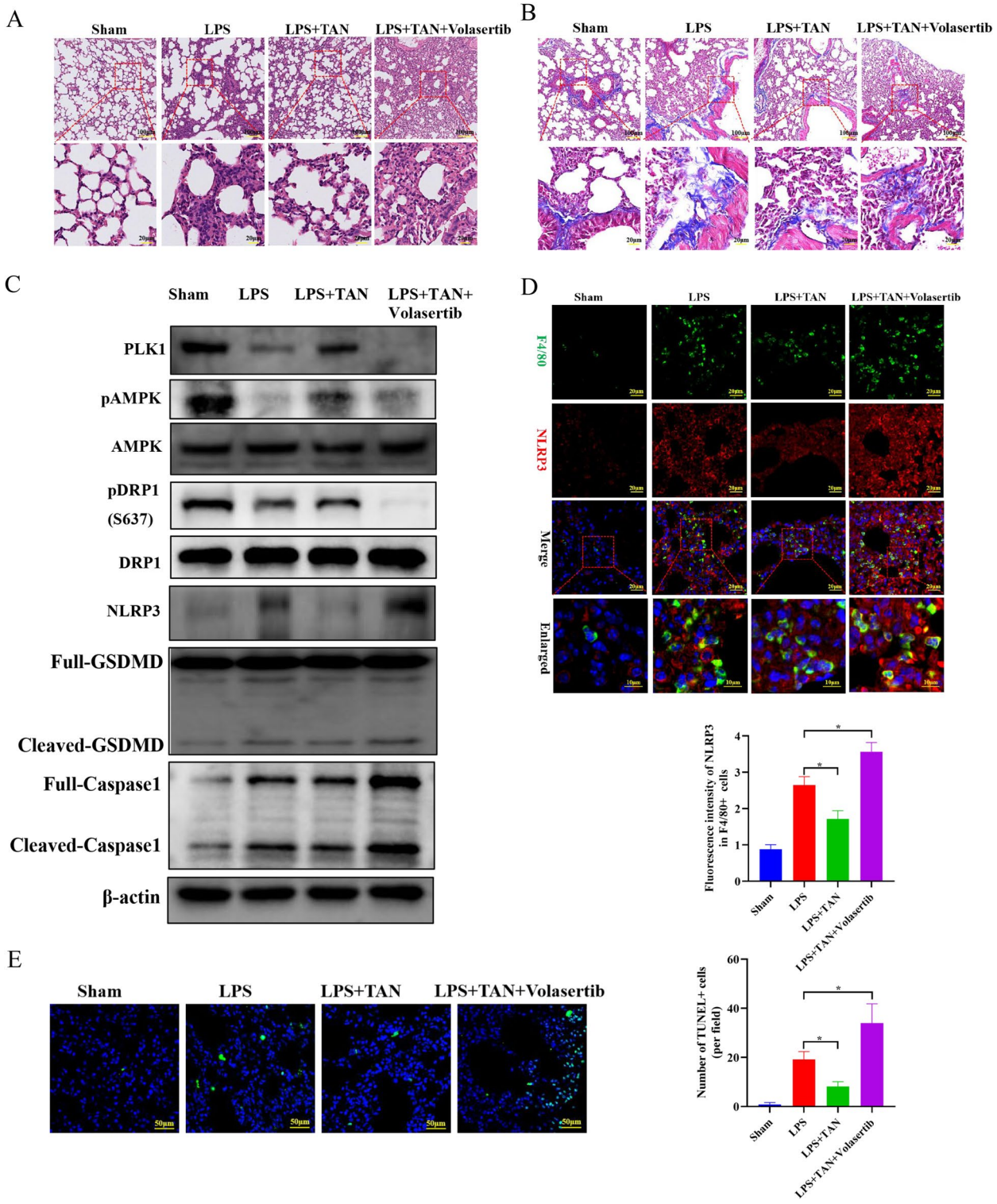

Fig. 8 TAN attenuates LPS-induced ALI in mice via regulating PLK1/AMPK/DRP1/NLRP3 signaling axis. **A** HE staining analysis of lung tissues. **B** Masson staining analysis of lung tissues. **C** Western blotting analysis of PLK1, pAMPK, AMPK, pDRP1, DRP1, NLRP3, GSDMD, and Caspase-1 protein expressions in the lung tissues ($n=3$). **D** Immunofluorescence staining analysis of the macrophage marker F4/80 (green) and NLRP3 (red) in the lung injury of all groups. Nucleus was stained with DAPI (blue). The quantification analysis of the immunofluorescence intensity of NLRP3 in the F4/80-positive cells in lung tissues ($n=6$). **E** Immunofluorescence staining analysis of the cellular apoptosis (green) in the lung injury of all groups. Nucleus was stained with DAPI (blue). The quantification analysis of apoptosis (green)-positive cells in lung tissues ($n=6$). Data are represented as mean ± SD, $^*p<0.05$ (color figure online)

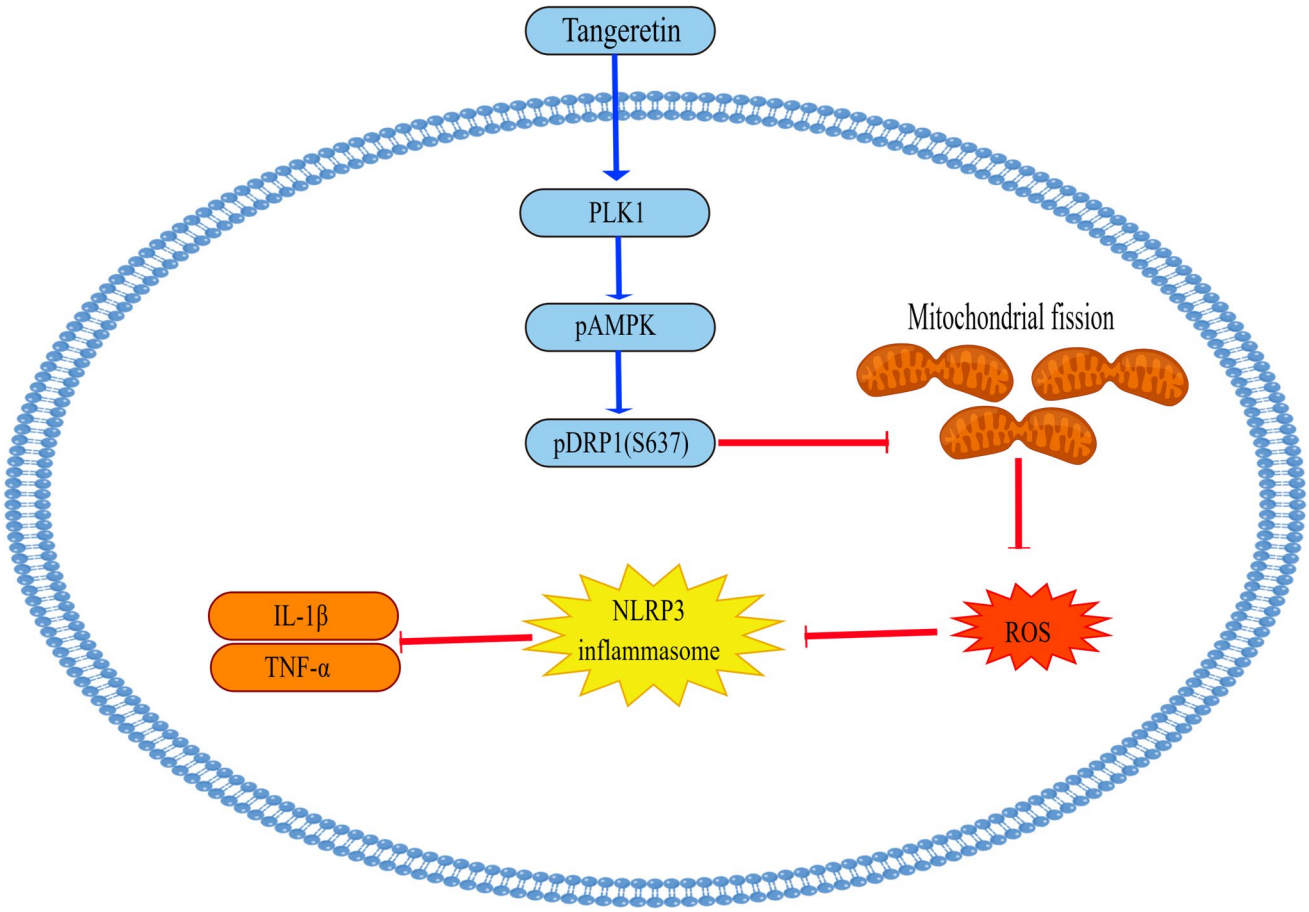

Fig. 9 Scheme summarizing the protective mechanism of TAN on LPS-induced ALI. TAN treatment significantly alleviated LPS-induced ALI by inhibiting ROS-mediated NLRP3 inflammasome activation via regulating PLK1/AMPK/DRP1 signaling axis

AMPK [45]. Thus, we speculate that TAN may protect mitochondrial morphology in sepsis-induced ALI through PLK1-AMPK-Drp1 axis. In the following experiments, we focused on PLK1.

TAN promotes PLK1-AMPK-Drp1 signaling in LPS-induced ALI in mice

Subsequently, we explored the effect of TAN on PLK1 expression in sepsis-induced ALI, and found that TAN treatment evidently increased PLK1 expression in the lung tissues, compared to that in the Sham group. Besides, PLK1 expression was significantly decreased in the LPS group, compared to those in the Sham group. Whereas, TAN treatment not only notably suppressed the LPS-induced reduction of PLK1 expression, but also increased AMPK phosphorylation and Drp1 phosphorylation (S637) in the LPS + TAN group, compared to the LPS group (Fig. 6A). Furthermore, immunofluorescence analysis also confirmed that TAN treatment significantly increased PLK1 expression and Drp1 phosphorylation (S637) in the lung tissues of the LPS + TAN group, compared to the LPS group (Fig. 6B, C). Taken together, these results indicate that TAN promotes PLK1-AMPK-Drp1 signaling in LPS-induced ALI in mice.

TAN suppresses NLRP3 inflammasome activation via regulating PLK1-Drp1 signaling in peritoneal macrophages stimulated with LPS and ATP

To explore whether the protective effect of TAN on sepsis-induced ALI was related to PLK1, LPS + ATP-stimulated peritoneal macrophages were pre-treated with the PLK1 inhibitor Volasertib or not. As shown in Fig. 7A, TAN treatment evidently inhibited LPS-induced reduction of PLK1 expression and Drp1 phosphorylation (S637), which was consistent with the result of in vivo (Fig. 6A). Besides, TAN treatment significantly suppressed LPS + ATP-induced NLRP3 expression, GSDMD and Caspase-1 activation (Fig. 6A). However, Volasertib treatment completely blocked the effects of TAN on PLK1 expression, Drp1 phosphorylation (S637), NLRP3 expression, and GSDMD and Caspase-1 activation in LPS + ATP-stimulated peritoneal

macrophages (Fig. 7A, B). In addition, Volasertib treatment also blocked the protective effects of TAN on the decline of mitochondrial membrane potential dysfunction and promotion of IL-1β and IL-18 mRNA expressions in LPS + ATP-stimulated peritoneal macrophages (Fig. 7C, D). Collectively, these results indicate that TAN suppresses NLRP3 inflammasome activation via regulating PLK1-Drp1 signaling in LPS + ATP-stimulated peritoneal macrophages.

TAN attenuates LPS-induced ALI in mice via regulating PLK1/AMPK/DRP1/NLRP3 signaling axis

We further investigated the protective mechanism of TAN on sepsis-induced ALI using LPS-stimulated mice pre-treated with the PLK1 inhibitor Volasertib or not. As shown in Fig. 8A, B, and supplementary Fig. 3, Volasertib treatment significantly abolished the protective effects of TAN on the lung pathologic injury and lung interstitial fibrosis in LPS-induced ALI in mice. Furthermore, Volasertib treatment blocked the effects of TAN on PLK1 expression, AMPK phosphorylation, Drp1 phosphorylation (S637), NLRP3 expression, GSDMD and Caspase-1 activation in LPS-induced lung injured tissues (Fig. 8C). Besides, immunofluorescence analysis also confirmed that Volasertib treatment blocked the protective effect of TAN on NLRP3 inflammasome activation in LPS-induced lung injured tissues (Fig. 8D). Moreover, TUNEL analysis showed that Volasertib treatment not only abolished the protective effect of TAN on cellular apoptosis in LPS-induced lung injured tissues, but also aggravated cellular apoptosis (Fig. 8E). Overall, these results suggest that TAN attenuates LPS-induced ALI in mice via regulating PLK1/AMPK/DRP1/ NLRP3 signaling axis.

Discussion

The present study firstly reveals an important role of TAN in alleviating sepsis-induced ALI. TAN administration efficiently inhibited pulmonary edema, reduced reducing pulmonary congestion, thickening of the alveolar wall and leukocyte accumulation, and suppressed inflammatory cytokine expression and inflammatory cell infiltration in sepsis-induced ALI in mice. Mechanistically, TAN suppresses excessive mitochondrial fission, ROS production, and NLRP3 inflammasome-mediated pyroptosis through activating PLK1/AMPK/DRP1 signaling pathway in sepsis-induced ALI (Fig. 9). Our study indicates TAN is a potentially therapeutic candidate against sepsis-induced ALI, and uncovers a novel potential target of TAN, and deepens our understanding on the protective mechanism of TAN on macrophage pyroptosis.

As is known that macrophage pyroptosis plays an essential role in the pathogenesis of sepsis-induced ALI via triggering excessive inflammatory responses [17, 18]. Inhibition of macrophage pyroptosis could efficiently alleviate sepsis-induced ALI [46]. TAN has been reported to suppress osteoarthritis, and renal failure through inhibiting inflammation via regulating NF-κB signaling [31, 47]. In this study, we found that TAN treatment significantly inhibited macrophage pyroptosis via decreasing NLRP3 expression, and GSDMD and Caspase-1 activation in the sepsis-induced ALI. These in vivo and in vitro data strongly support the beneficial role of TAN on macrophage pyroptosis and sepsis-induced ALI.

ROS is known as a prominent stimulator to trigger the activation of NLRP3 inflammasome [48, 49], and dysfunction of mitochondrial fusion and fission produces amounts of ROS [50]. It is well accepted that Drp1 is a main promotor of mitochondrial fission [51], and phosphorylation at Ser-637 inhibits Drp1 activity while phosphorylation at Ser-616 activates Drp1 activity [52]. Previous study reported quercetin protected ethanol-induced hepatocyte pyroptosis through inhibiting ROS-NLRP3 signaling axis via promoting mitochondrial homeostasis [53]. Nodakenin attenuates knee osteoarthritis by regulating mitochondrial Drp1/ROS/NLRP3 axis [54]. Similar to these studies, our study found that TAN treatment could notably restored mitochondrial morphology, and inhibited excessive mitochondrial fission and ROS accumulation in the lung tissue with sepsis-induced ALI. Nowadays, Ser-637 of Drp1 has been reported to be phosphorylated by a kinase anchoring protein 1 (AKAP1) [55], and AMPK [42]. In this study, our study for the first time identified PLK1 is a potential target of TAN via bioinformatic analysis and molecular docking, and TAN alleviated sepsis-induced ALI through inhibiting ROS-mediated NLRP3 inflammasome activation via regulating PLK1/AMPK/DRP1 (S637) signaling axis. Inhibiting PLK1 via Volasertib evidently blocked the promotive effects of TAN on the AMPK/DRP1(S637) signaling axis, and aggravated NLRP3 inflammasome activation in the lung tissue of septic mice. Besides, phosphorylation at Ser-637, Drp1 could also be phosphorylated at Ser-616 by the cyclin-dependent kinase (CDK) family [56], extracellular-signal-regulated kinase1/2 (ERK1/2) [57], and PKCδ [58]. Previous studies found that TAN inhibited ERK1/2 phosphorylation in a dose-dependent manner in human T47D mammary cancer cells [59], and in human glomerular mesangial cells [60]. Whether the protective role of TAN on macrophage pyroptosis and sepsis-induced ALI is also related to regulate ERK1/2/Drp1(S616) needs to be clarified in the following studies.

In addition to PLK1, our study also identified CDK1 was another potential target of TAN for treating sepsis-induced ALI. CDK1 is reported to promote cell cycle progression through the G2/M phase transition and activate homologous recombination DNA repair pathway [61]. CDK1 is highly

expressed in several tumors, such as lung cancer, gastric cancer, and cervical cancer, and functions to promote the stemness of cancer cells, cell proliferation, and cell migration [62–64]. Given that CDK1 could phosphorylate Drp1 at Ser-616 [58], and phosphorylation at Ser-637 inhibits Drp1 activity [52], we speculate that the protective effect of TAN on macrophage pyroptosis and sepsis-induced ALI is also related to regulate CDK1/Drp1(S616) signaling axis, which needs to be investigated in the following studies.

In conclusion, our study indicates TAN attenuates sepsis-induced ALI by inhibiting ROS-mediated NLRP3 inflammasome activation via regulating PLK1/AMPK/DRP1 signaling axis, and TAN is a potentially therapeutic candidate against ALI through inhibiting pyroptosis.

Supplementary Information The online version contains supplementary material available at https://doi.org/10.1007/s00011-023-01819-8.

Author contributions Conceptualization, YL, YZ, ZS, BD, JZ, and ZZ; data curation, YL, YZ, GY, DZ, ZH, WG; methodology, YL, YZ, GY, DZ, ZH, WG; resources, BD, JZ, and ZZ; supervision, KA, ZS, BD, JZ, and ZZ; validation, YL, YZ, GY, DZ, ZH, WG; writing-original draft, YL, YZ, GY, DZ, ZH, WG, BD, JZ; writing-review and editing, YL, KA, ZS, BD, JZ, and ZZ. All authors have read and agreed to the published version of the manuscript.

Funding This study was supported by the National Natural Science Foundation of China (82004317), Guangzhou Science and Technology Plan Project (202102010322), and Guangdong Bureau of Traditional Chinese Medicine Project (20241115).

Data availability statement All data generated or analyzed during this study are included in this published article and its supplementary information files.

Declarations

Conflict of interest The authors declare that there is no conflict of interest.

Institutional review board statement All animal procedures were reviewed and approved by the Institutional Animal Care and Use Committee of Guangdong Provincial Hospital of Traditional Chinese Medicine (No. 2023017).

Informed consent Not applicable.

References

1. Vincent JL. Current sepsis therapeutics. EBioMedicine. 2022;86: 104318. https://doi.org/10.1016/j.ebiom.2022.104318.
2. Dartiguelongue JB. Systemic inflammation and sepsis part II: functional consequences of the storm. Arch Argent Pediatr. 2021;119:e1–10. https://doi.org/10.5546/aap.2021.eng.e1.
3. Chousterman BG, Swirski FK, Weber GF. Cytokine storm and sepsis disease pathogenesis. Semin Immunopathol. 2017;39:517–28. https://doi.org/10.1007/s00281-017-0639-8.
4. Perner A, Gordon AC, De Backer D, Dimopoulos G, Russell JA, Lipman J, Jensen JU, Myburgh J, Singer M, Bellomo R, Walsh T. Sepsis: frontiers in diagnosis, resuscitation and antibiotic therapy. Intensive Care Med. 2016;42:1958–69. https://doi.org/10.1007/s00134-016-4577-z.
5. Kaku S, Nguyen CD, Htet NN, Tutera D, Barr J, Paintal HS, Kuschner WG. Acute respiratory distress syndrome: etiology, pathogenesis, and summary on management. J Intensive Care Med. 2020;35:723–37. https://doi.org/10.1177/0885066619855021.
6. Fan EKY, Fan J. Regulation of alveolar macrophage death in acute lung inflammation. Respir Res. 2018;19:50. https://doi.org/10.1186/s12931-018-0756-5.
7. Arora S, Dev K, Agarwal B, Das P, Syed MA. Macrophages: their role, activation and polarization in pulmonary diseases. Immunobiology. 2018;223:383–96. https://doi.org/10.1016/j.imbio.2017.11.001.
8. Chen R, Cao C, Liu H, Jiang W, Pan R, He H, Ding K, Meng Q. Macrophage Sprouty4 deficiency diminishes sepsis-induced acute lung injury in mice. Redox Biol. 2022;58: 102513. https://doi.org/10.1016/j.redox.2022.102513.
9. Jiang W, Ma C, Bai J, Du X. Macrophage SAMSN1 protects against sepsis-induced acute lung injury in mice. Redox Biol. 2022;56: 102432. https://doi.org/10.1016/j.redox.2022.102432.
10. Chen Q, Shao X, He Y, Lu E, Zhu L, Tang W. Norisoboldine attenuates sepsis-induced acute lung injury by modulating macrophage polarization via PKM2/HIF-1alpha/PGC-1alpha pathway. Biol Pharm Bull. 2021;44:1536–47. https://doi.org/10.1248/bpb.b21-00457.
11. Fu Y, Wang D, Wang S, Zhang Q, Liu H, Yang S, Xu Y, Ying B. Blockade of macrophage-associated programmed death 1 inhibits the pyroptosis signalling pathway in sepsis. Inflamm Res Off J Eur Histamine Res Soc. 2021;70:993–1004. https://doi.org/10.1007/s00011-021-01493-8.
12. Zhuo Y, Yang L, Li D, Zhang L, Zhang Q, Zhang S, Li C, Cui L, Hao J, Li J, Wang X. Syringaresinol resisted sepsis-induced acute lung injury by suppressing pyroptosis via the oestrogen receptor-beta signalling pathway. Inflammation. 2022;45:824–37. https://doi.org/10.1007/s10753-021-01587-9.
13. Wang J, Li J, Lou A, Lin Y, Xu Q, Cui W, Huang W, Wang G, Li Y, Sun J, Gong J, Guo Q, Qiu H, Meng Y, Li X. Sacubitril/valsartan alleviates sepsis-induced acute lung injury via inhibiting GSDMD-dependent macrophage pyroptosis in mice. FEBS J. 2023;290:2180–98. https://doi.org/10.1111/febs.16696.
14. Sun L, Ma W, Gao W, Xing Y, Chen L, Xia Z, Zhang Z, Dai Z. Propofol directly induces caspase-1-dependent macrophage pyroptosis through the NLRP3-ASC inflammasome. Cell Death Dis. 2019;10:542. https://doi.org/10.1038/s41419-019-1761-4.
15. Yu P, Zhang X, Liu N, Tang L, Peng C, Chen X. Pyroptosis: mechanisms and diseases. Signal Transduct Target Ther. 2021;6:128. https://doi.org/10.1038/s41392-021-00507-5.
16. Feng Y, Li M, Yangzhong X, Zhang X, Zu A, Hou Y, Li L, Sun S. Pyroptosis in inflammation-related respiratory disease. J Physiol Biochem. 2022;78:721–37. https://doi.org/10.1007/s13105-022-00909-1.
17. Jiao Y, Zhang T, Zhang C, Ji H, Tong X, Xia R, Wang W, Ma Z, Shi X. Exosomal miR-30d-5p of neutrophils induces M1 macrophage polarization and primes macrophage pyroptosis in sepsis-related acute lung injury. Crit Care. 2021;25:356. https://doi.org/10.1186/s13054-021-03775-3.
18. Xu Z, Li D, Qu W, Yin Y, Qiao S, Zhu Y, Shen S, Hou Y, Yang J, Wang T. Card9 protects sepsis by regulating Ripk2-mediated activation of NLRP3 inflammasome in macrophages. Cell Death Dis. 2022;13:502. https://doi.org/10.1038/s41419-022-04938-y.

19. Liu Q, Zhang D, Hu D, Zhou X, Zhou Y. The role of mitochondria in NLRP3 inflammasome activation. Mol Immunol. 2018;103:115–24. https://doi.org/10.1016/j.molimm.2018.09.010.
20. Bertholet AM, Delerue T, Millet AM, Moulis MF, David C, Daloyau M, Arnaune-Pelloquin L, Davezac N, Mils V, Miquel MC, Rojo M, Belenguer P. Mitochondrial fusion/fission dynamics in neurodegeneration and neuronal plasticity. Neurobiol Dis. 2016;90:3–19. https://doi.org/10.1016/j.nbd.2015.10.011.
21. Giacomello M, Pyakurel A, Glytsou C, Scorrano L. The cell biology of mitochondrial membrane dynamics. Nat Rev Mol Cell Biol. 2020;21:204–24. https://doi.org/10.1038/s41580-020-0210-7.
22. Quintana-Cabrera R, Scorrano L. Determinants and outcomes of mitochondrial dynamics. Mol Cell. 2023;83:857–76. https://doi.org/10.1016/j.molcel.2023.02.012.
23. Serasinghe MN, Chipuk JE. Mitochondrial fission in human diseases. Handb Exp Pharmacol. 2017;240:159–88. https://doi.org/10.1007/164_2016_38.
24. Gao S, Hu J. Mitochondrial fusion: the machineries in and out. Trends Cell Biol. 2021;31:62–74. https://doi.org/10.1016/j.tcb.2020.09.008.
25. Mohsin M, Tabassum G, Ahmad S, Ali S, Ali Syed M. The role of mitophagy in pulmonary sepsis. Mitochondrion. 2021;59:63–75. https://doi.org/10.1016/j.mito.2021.04.009.
26. Shi J, Yu T, Song K, Du S, He S, Hu X, Li X, Li H, Dong S, Zhang Y, Xie Z, Li C, Yu J. Dexmedetomidine ameliorates endotoxin-induced acute lung injury in vivo and in vitro by preserving mitochondrial dynamic equilibrium through the HIF-1a/HO-1 signaling pathway. Redox Biol. 2021;41: 101954. https://doi.org/10.1016/j.redox.2021.101954.
27. Zhao N, Sun R, Cui Y, Song Y, Ma W, Li Y, Liang J, Wang G, Yu Y, Han J, Xie K. High concentration hydrogen mitigates sepsis-induced acute lung injury in mice by alleviating mitochondrial fission and dysfunction. J Pers Med. 2023. https://doi.org/10.3390/jpm13020244.
28. Li G, Fu T, Wang W, Xiong R, Liu B, He R, Xu C, Wang W, Li N, Geng Q. Pretreatment with Kahweol attenuates sepsis-induced acute lung injury via improving mitochondrial homeostasis in a CaMKKII/AMPK-dependent pathway. Mol Nutr Food Res. 2023. https://doi.org/10.1002/mnfr.202300083.
29. Xu JJ, Liu Z, Tang W, Wang GC, Chung HY, Liu QY, Zhuang L, Li MM, Li YL. Tangeretin from citrus reticulate inhibits respiratory syncytial virus replication and associated inflammation in vivo. J Agric Food Chem. 2015;63:9520–7. https://doi.org/10.1021/acs.jafc.5b03482.
30. Ashrafizadeh M, Ahmadi Z, Mohammadinejad R, Ghasemipour Afshar E. Tangeretin: a mechanistic review of its pharmacological and therapeutic effects. J Basic Clin Physiol Pharmacol. 2020. https://doi.org/10.1515/jbcpp-2019-0191.
31. Shi Y, Chen J, Li S, Wu Y, Yu C, Ni L, Xiao J, Shao Z, Zhu H, Wang J, Wang X, Zhang X. Tangeretin suppresses osteoarthritis progression via the Nrf2/NF-kappaB and MAPK/NF-kappaB signaling pathways. Phytomed Int J Phytother Phytopharmacol. 2022;98: 153928. https://doi.org/10.1016/j.phymed.2022.153928.
32. Ke Z, Tan S, Li H, Jiang S, Li Y, Chen R, Li M. Tangeretin improves hepatic steatosis and oxidative stress through the Nrf2 pathway in high fat diet-induced nonalcoholic fatty liver disease mice. Food Funct. 2022;13:2782–90. https://doi.org/10.1039/d1fo02989d.
33. Shiroorkar PN, Afzal O, Kazmi I, Al-Abbasi FA, Altamimi ASA, Gubbiyappa KS, Sreeharsha N. Cardioprotective effect of tangeretin by inhibiting PTEN/AKT/mTOR axis in experimental sepsis-induced myocardial dysfunction. Molecules. 2020. https://doi.org/10.3390/molecules25235622.
34. Li M, Zhao Y, Qi D, He J, Wang D. Tangeretin attenuates lipopolysaccharide-induced acute lung injury through Notch signaling pathway via suppressing Th17 cell response in mice. Microb Pathog. 2020;138: 103826. https://doi.org/10.1016/j.micpath.2019.103826.
35. Zan J, Xu R, Tang X, Lu M, Xie S, Cai J, Huang Z, Zhang J. RNA helicase DDX5 suppresses IFN-I antiviral innate immune response by interacting with PP2A-Cbeta to deactivate IRF3. Exp Cell Res. 2020;396: 112332. https://doi.org/10.1016/j.yexcr.2020.112332.
36. Luo Q, Liu R, Qu K, Liu G, Hang M, Chen G, Xu L, Jin Q, Guo D, Kang Q. Cangrelor ameliorates CLP-induced pulmonary injury in sepsis by inhibiting GPR17. Eur J Med Res. 2021;26:70. https://doi.org/10.1186/s40001-021-00536-4.
37. Mikawa K, Nishina K, Takao Y, Obara H. ONO-1714, a nitric oxide synthase inhibitor, attenuates endotoxin-induced acute lung injury in rabbits. Anesth Analg. 2003;97:1751–5. https://doi.org/10.1213/01.ANE.0000086896.90343.13.
38. Yu Z, Zheng L, Geng Y, Zhang Y, Wang Y, You G, Cai M, Li M, Cheng X, Zan J. FTO alleviates cerebral ischemia/reperfusion-induced neuroinflammation by decreasing cGAS mRNA stability in an m6A-dependent manner. Cell Signal. 2023;109: 110751. https://doi.org/10.1016/j.cellsig.2023.110751.
39. Fan H, Cui J, Liu F, Zhang W, Yang H, He N, Dong Z, Dong J. Malvidin protects against lipopolysaccharide-induced acute liver injury in mice via regulating Nrf2 and NLRP3 pathways and suppressing apoptosis and autophagy. Eur J Pharmacol. 2022;933: 175252. https://doi.org/10.1016/j.ejphar.2022.175252.
40. Li Z, Liu T, Feng Y, Tong Y, Jia Y, Wang C, Cui R, Qu K, Liu C, Zhang J. PPARgamma alleviates sepsis-induced liver injury by inhibiting hepatocyte pyroptosis via inhibition of the ROS/TXNIP/NLRP3 signaling pathway. Oxid Med Cell Longev. 2022;2022:1269747. https://doi.org/10.1155/2022/1269747.
41. Andreyev AY, Kushnareva YE, Starkov AA. Mitochondrial metabolism of reactive oxygen species. Biochem Biokhimiia. 2005;70:200–14. https://doi.org/10.1007/s10541-005-0102-7.
42. Wang PW, Pang Q, Zhou T, Song XY, Pan YJ, Jia LP, Zhang AH. Irisin alleviates vascular calcification by inhibiting VSMC osteoblastic transformation and mitochondria dysfunction via AMPK/Drp1 signaling pathway in chronic kidney disease. Atherosclerosis. 2022;346:36–45. https://doi.org/10.1016/j.atherosclerosis.2022.02.007.
43. Du J, Li H, Song J, Wang T, Dong Y, Zhan A, Li Y, Liang G. AMPK activation alleviates myocardial ischemia-reperfusion injury by regulating Drp1-mediated mitochondrial dynamics. Front Pharmacol. 2022;13: 862204. https://doi.org/10.3389/fphar.2022.862204.
44. Zhang Y, Song Y, Wang C, Jiang J, Liu S, Bai Q, Li L, Jin H, Jin Y, Yan G. Panax notoginseng saponin R1 attenuates allergic rhinitis through AMPK/Drp1 mediated mitochondrial fission. Biochem Pharmacol. 2022;202: 115106. https://doi.org/10.1016/j.bcp.2022.115106.
45. Hu HJ, Wang XH, Zhang TQ, Liu Y, Chen ZR, Zhang ZZ, Huang H, Tang HF, Jiang ZS. PLK1 promotes cholesterol efflux and alleviates atherosclerosis by up-regulating ABCA1 and ABCG1 expression via the AMPK/PPARgamma/LXRalpha pathway. Biochim Biophys Acta Mol Cell Biol Lipids. 2022;1867: 159221. https://doi.org/10.1016/j.bbalip.2022.159221.
46. Kang R, Zeng L, Zhu S, Xie Y, Liu J, Wen Q, Cao L, Xie M, Ran Q, Kroemer G, Wang H, Billiar TR, Jiang J, Tang D. Lipid peroxidation drives gasdermin D-mediated pyroptosis in lethal polymicrobial sepsis. Cell Host Microbe. 2018;24:97–108. https://doi.org/10.1016/j.chom.2018.05.009. (**e104**).
47. Wu J, Zhao YM, Deng ZK. Tangeretin ameliorates renal failure via regulating oxidative stress, NF-kappaB-TNF-alpha/iNOS signalling and improves memory and cognitive deficits in 5/6 nephrectomized rats. Inflammopharmacology. 2018;26:119–32. https://doi.org/10.1007/s10787-017-0394-4.

48. Cai SM, Yang RQ, Li Y, Ning ZW, Zhang LL, Zhou GS, Luo W, Li DH, Chen Y, Pan MX, Li X. Angiotensin-(1–7) improves liver fibrosis by regulating the NLRP3 inflammasome via redox balance modulation. Antioxid Redox Signal. 2016;24:795–812. https://doi.org/10.1089/ars.2015.6498.
49. Minutoli L, Puzzolo D, Rinaldi M, Irrera N, Marini H, Arcoraci V, Bitto A, Crea G, Pisani A, Squadrito F, Trichilo V, Bruschetta D, Micali A, Altavilla D. ROS-mediated NLRP3 inflammasome activation in brain, heart kidney testis ischemia reperfusion injury. Oxid Med Cell Longev. 2016;2016:2183026. https://doi.org/10.1155/2016/2183026.
50. Jezek J, Cooper KF, Strich R. The impact of mitochondrial fission-stimulated ROS production on pro-apoptotic chemotherapy. Biology (Basel). 2021. https://doi.org/10.3390/biology10010033.
51. Hu C, Huang Y, Li L. Drp1-dependent mitochondrial fission plays critical roles in physiological and pathological progresses in mammals. Int J Mol Sci. 2017. https://doi.org/10.3390/ijms18010144.
52. Gomes LC, Di Benedetto G, Scorrano L. During autophagy mitochondria elongate, are spared from degradation and sustain cell viability. Nat Cell Biol. 2011;13:589–98. https://doi.org/10.1038/ncb2220.
53. Zhao X, Wang C, Dai S, Liu Y, Zhang F, Peng C, Li Y. Quercetin protects ethanol-induced hepatocyte pyroptosis via scavenging mitochondrial ROS and promoting PGC-1alpha-regulated mitochondrial homeostasis in L02 cells. Oxid Med Cell Longev. 2022;2022:4591134. https://doi.org/10.1155/2022/4591134.
54. Yi N, Mi Y, Xu X, Li N, Chen B, Yan K, Tan K, Zhang B, Wang L, Kuang G, Lu M. Nodakenin attenuates cartilage degradation and inflammatory responses in a mice model of knee osteoarthritis by regulating mitochondrial Drp1/ROS/NLRP3 axis. Int Immunopharmacol. 2022;113: 109349. https://doi.org/10.1016/j.intimp.2022.109349.
55. Merrill RA, Dagda RK, Dickey AS, Cribbs JT, Green SH, Usachev YM, Strack S. Mechanism of neuroprotective mitochondrial remodeling by PKA/AKAP1. PLoS Biol. 2011;9: e1000612. https://doi.org/10.1371/journal.pbio.1000612.
56. Strack S, Wilson TJ, Cribbs JT. Cyclin-dependent kinases regulate splice-specific targeting of dynamin-related protein 1 to microtubules. J Cell Biol. 2013;201:1037–51. https://doi.org/10.1083/jcb.201210045.
57. Prieto J, Leon M, Ponsoda X, Sendra R, Bort R, Ferrer-Lorente R, Raya A, Lopez-Garcia C, Torres J. Early ERK1/2 activation promotes DRP1-dependent mitochondrial fission necessary for cell reprogramming. Nat Commun. 2016;7:11124. https://doi.org/10.1038/ncomms11124.
58. Zaja I, Bai X, Liu Y, Kikuchi C, Dosenovic S, Yan Y, Canfield SG, Bosnjak ZJ. Cdk1, PKCdelta and calcineurin-mediated Drp1 pathway contributes to mitochondrial fission-induced cardiomyocyte death. Biochem Biophys Res Commun. 2014;453:710–21. https://doi.org/10.1016/j.bbrc.2014.09.144.
59. Van Slambrouck S, Parmar VS, Sharma SK, De Bondt B, Fore F, Coopman P, Vanhoecke BW, Boterberg T, Depypere HT, Leclercq G, Bracke ME. Tangeretin inhibits extracellular-signal-regulated kinase (ERK) phosphorylation. FEBS Lett. 2005;579:1665–9. https://doi.org/10.1016/j.febslet.2004.10.114.
60. Chen F, Ma Y, Sun Z, Zhu X. Tangeretin inhibits high glucose-induced extracellular matrix accumulation in human glomerular mesangial cells. Biomed Pharmacother (Biomedecine & pharmacotherapie). 2018;102:1077–83. https://doi.org/10.1016/j.biopha.2018.03.169.
61. Sunada S, Saito H, Zhang D, Xu Z, Miki Y. CDK1 inhibitor controls G2/M phase transition and reverses DNA damage sensitivity. Biochem Biophys Res Commun. 2021;550:56–61. https://doi.org/10.1016/j.bbrc.2021.02.117.
62. Huang Z, Shen G, Gao J. CDK1 promotes the stemness of lung cancer cells through interacting with Sox2. Clin Transl Oncol Off Publ Fed Span Oncol Soc Natl Cancer Inst Mexico. 2021;23:1743–51. https://doi.org/10.1007/s12094-021-02575-z.
63. Li FN, Zhang QY, Li O, Liu SL, Yang ZY, Pan LJ, Zhao C, Gong W, Shu YJ, Dong P. ESRRA promotes gastric cancer development by regulating the CDC25C/CDK1/CyclinB1 pathway via DSN1. Int J Biol Sci. 2021;17:1909–24. https://doi.org/10.7150/ijbs.57623.
64. Tang J, Pan H, Wang W, Qi C, Gu C, Shang A, Zhu J. MiR-495-3p and miR-143-3p co-target CDK1 to inhibit the development of cervical cancer. Clin Transl Oncol Off Publ Fed Span Oncol Soc Natl Cancer Inst Mexico. 2021;23:2323–34. https://doi.org/10.1007/s12094-021-02687-6.

Authors and Affiliations

Yuntao Liu[1] · Yuting Zhang[2] · Guoxing You[2] · Danwen Zheng[1] · Zhipeng He[1] · Wenjie Guo[2] · Kim Antonina[3] · Ziyadullaev Shukhrat[3] · Banghan Ding[1] · Jie Zan[2] · Zhongde Zhang[1]

✉ Banghan Ding
banghanding@139.com

✉ Jie Zan
zanj@gdut.edu.cn

✉ Zhongde Zhang
doctorzzd99@163.com

[1] State Key Laboratory of Traditional Chinese Medicine Syndrom , The second Affiliated Hospital of Guangzhou University of Chinese Medicine, Guangzhou 510120, China

[2] School of Biomedical and Pharmaceutical Sciences, Guangdong University of Technology, Guangzhou 510006, China

[3] No. 1 Department of Internal Diseases, Samarkand State Medical University, Samarkand, Uzbekistan